

Highlights

Wave Sequential Data Assimilation in Support of Wave Energy Converter Power Prediction

Mohammad Khalil, Carlos Michelén Ströfer, Kaustubha Raghukumar, Ann Dallman

- Developed a data assimilation framework that leverages numerical spectral wave models for forecasting and the ensemble Kalman filter for data assimilation of near-shore wave spectra
- Developed data-driven error models that aim to capture the discrepancy in prescribed boundary conditions of wave spectra
- Assimilated real data obtained offshore Yakutat, Alaska, from low-cost wave measurement buoys, resulting in improved forecast skill in comparison to traditional numerical forecasts.

Wave Sequential Data Assimilation in Support of Wave Energy Converter Power Prediction

Mohammad Khalil^a, Carlos Michelén Ströfer^b, Kaustubha Raghukumar^c and Ann Dallman^b

^a*Sandia National Laboratories, Livermore, California, 94551, USA*

^b*Sandia National Laboratories, Albuquerque, New Mexico, 87185, USA*

^c*Integral Consulting Inc., Santa cruz, California, 95060, USA*


ABSTRACT

Integration of renewable power sources into grids remains an active research and development area, particularly for less developed renewable energy technologies such as wave energy converters (WECs). WECs are projected to have strong early market penetration for remote communities, which serve as natural microgrids. Hence, accurate wave predictions to manage the interactions of a WEC array with microgrids is especially important. Recently developed, low-cost wave measurement buoys allow for operational assimilation of wave data at remote, site specific locations where real-time data have previously been unavailable.

We present the development and assessment of a wave modeling framework with real-time data assimilation capabilities for WEC power prediction. The availability of real-time wave spectra from low-cost wave measurement buoys allows for operational data assimilation with the ensemble Kalman filter technique within a hybrid modeling procedure whereby physics-based numerical wave models are combined with data-driven error models that aim to capture the discrepancy in prescribed boundary conditions. With that aim, measured wave spectra are assimilated for combined state and parameter estimation while taking into account model and observational errors. The analysis allows for more accurate and precise wave characteristic predictions at the locations of interest. Initial deployment data obtained offshore Yakutat, Alaska, indicated that measured wave data from one buoy that were assimilated into the wave modeling framework resulted in improved forecast skill in comparison to traditional numerical forecasts.

1. Introduction

A number of different wave energy converter (WEC) technologies are currently being developed to harness this largely untapped energy resource; however successful incorporation of wave energy projects to electric grids requires (1) forecasting available energy, (2) efficiently harnessing that energy (via multiple devices in a “farm” or array), and (3) modular management of sources, loads, and storage. Integration of renewable power sources into electrical grids remains an active research and development area, particularly for less developed renewable energy technologies such

 mkhalil@sandia.gov (M. Khalil)

ORCID(s): 0000-0001-6579-7127 (M. Khalil)

as WECs. Effective grid management will require accurate and precise forecasts, particularly for high penetrations of renewables onto microgrids. Typical wave sea state forecasting has significant errors, which will compound when coupled with array power output. Further, understanding uncertainty of the power forecast (i.e., the forecast model for wave power produced by a WEC array with and without improvements to incoming wave sea state forecasting) is critical to quantify and reduce. In this investigation, we provide a framework that couples data assimilation with wave forecasting in order to arrive at more accurate and certain wave forecasts. These forecasts will enable future efforts to balance energy variability on electrical grids to obtain energy resiliency and security, and to ensure that the potential of ocean wave energy is realized. This is enabled by the availability of low-cost wave measurement buoys.

Recently, a data assimilation framework utilized SWAN to predict wave characteristics in the basin of the Black Sea [Rusu and Raileanu (2016)] and the Portuguese coastal area [Guedes Soares, Rusu, Bernardino and Pilar (2011)]. Both of those approaches rely on extrapolating the difference between the measured data and simulation results and applying corrections at the boundaries of the computational domain. In this investigation, we will update the boundary conditions using state-of-the-art data assimilation strategies. Furthermore, our corrections will be non-linear-in-time versus ones that are linear-in-time as applied in [Rusu and Raileanu (2016); Guedes Soares et al. (2011)].

In the context of sequential data assimilation for real-time applications, Kalman Filter (KF) has been widely applied to estimate the statistical moments of the system state vector given noisy observational data [Kalman (1960)], providing optimal estimates for such statistics in the case of linear systems with additive Gaussian noise. For nonlinear systems, Monte Carlo based sequential filtering algorithms have gained popularity due to their wide scope of applicability. These sampling-based methods represent the probability density function (pdf) of the state vector using a finite number of possible states or trajectories. The two most popular classes of Monte Carlo based filters are the Ensemble Kalman Filter (EnKF) [Evensen (2006)] and Particle Filter (PF) [Tanizaki (1996); Doucet, Godsill and Andrieu (2000); Ristic, Arulampalam and Gordon (2004)]. EnKF and PF can be easily applied to complicated black-box models with no access to derivative information (as is the case for the SWAN numerical wave model).

In addition to estimating the unknown state from noisy observations, we will attempt to correct pre-specified boundary conditions using time-varying error models, whose unknown parameters will also be inferred from the available data. One popular approach to solving the parameter estimation problem within sequential data assimilation settings involves augmenting the state vector with the unknown system parameters. The new augmented state vector is estimated using EnKF in the same manner that the original state vector is estimated. The parameter space is only explored at the initialization of the algorithm according to the prior pdf of the unknown parameters [Andrieu and Doucet (2003)], with performance tightly related to the choice of priors. For poorly selected prior, the filtering algorithms fail after a few assimilation cycles, a phenomenon commonly known as filter divergence. Unfortunately, in our setting the parameters belong to a purely data-driven model, making it more difficult to provide a sufficiently compact prior pdf ahead of the assimilation experiment. To alleviate this problem, the parameters are perturbed by artificial noise in time to achieve convergence of the filtering algorithm [Kitagawa (1998); Khalil, Sarkar and Adhikari (2009)].

The paper is organized as follows. In Section 2, we provide an overview of joint state and parameter inference of dynamical systems using the ensemble Kalman filter for sequential data

assimilation. In Section 3, we present an application of the novel data assimilation workflows to a case study involving an area offshore of Yakutat, Alaska, with results and discussions provided in Section 4. We conclude, in Section 5, with a summary of our findings and some additional observations in the context of future work.

2. Sequential Data Assimilation

In this section, we provide an overview of the ensemble Kalman filter (EnKF) as a sequential data assimilation technique for the joint inference of unknown state and parameters of dynamical systems.

2.1. State-Space Representation of Discrete Dynamical Systems

In a data assimilation setting, the model and measurement equations for a discrete state-space representation of a (nonlinear) dynamical system are given by [Evensen et al. (2009)]

$$\mathbf{u}_{k+1} = \mathbf{g}(\mathbf{u}_k, \mathbf{f}_k, \boldsymbol{\theta}, \boldsymbol{\epsilon}_k) , \quad (1)$$

$$\mathbf{d}_j = \mathbf{H} \mathbf{u}_{k(j)} + \boldsymbol{\epsilon}_j . \quad (2)$$

Here \mathbf{u}_k is the unknown state vector at time instance $t = t_k$, \mathbf{g} is the discrete vector-valued nonlinear model operator, $\boldsymbol{\phi}$ is the vector of unknown (or weakly known) modeling parameters, \mathbf{f} is a vector of deterministic (i.e. known) inputs, $\boldsymbol{\epsilon}_k$ is a random vector to capture modeling uncertainties, and \mathbf{d} , the measurement vector, relates to the true state through the linear measurement operator \mathbf{H} with $\boldsymbol{\epsilon}_j$ being a random vector that captures the additive observational errors/uncertainties. Note that this can be extended to handle non-linear measurement operators (see [Evensen et al. (2009)] for details). The indices k and $k(j)$ denotes the time steps for state evolution and arrival of measurement data, respectively.

2.2. Joint State and Parameter Estimation

In the framework of nonlinear filtering, one popular strategy to infer the unknown parameter vector $\boldsymbol{\theta}$ along with the state is to treat the parameters as a time-varying quantities, artificially perturbed randomly to avoid filter divergence (e.g. [Chui and Chen (1999); Khalil et al. (2009)]). In this case, the state space model can be written as

$$\mathbf{u}_{k+1} = \mathbf{g}(\mathbf{u}_k, \mathbf{f}_k, \boldsymbol{\theta}_k, \boldsymbol{\epsilon}_k) , \quad (3)$$

$$\boldsymbol{\theta}_{k+1} = \boldsymbol{\theta}_k + \boldsymbol{\xi}_k , \quad (4)$$

$$(5)$$

where $\boldsymbol{\xi}$ is usually chosen to be a multivariate normal random vector that artificially inflates the variance (uncertainty) of the unknown parameter vector to avoid filter divergence. The *augmented* state vector is formed by appending the unknown parameter vector to the original state vector leading to the following augmented state space model:

$$\mathbf{x}_{k+1} = \mathbb{G}(\mathbf{x}_k, \mathbf{f}_k, \boldsymbol{\zeta}_k) , \quad (6)$$

$$\mathbf{d}_j = \mathbb{H} \mathbf{x}_{k(j)} + \boldsymbol{\epsilon}_j . \quad (7)$$

where

$$\mathbf{x}_k = \begin{Bmatrix} \mathbf{u}_k \\ \boldsymbol{\theta}_k \end{Bmatrix}; \quad \boldsymbol{\zeta}_k = \begin{Bmatrix} \boldsymbol{\varepsilon}_k \\ \boldsymbol{\xi}_k \end{Bmatrix} \quad (8)$$

Nonlinear filter can provide estimates of the conditional distribution of the uncertain state \mathbf{u} and parameters $\boldsymbol{\theta}$ given noisy observations \mathbf{d} . In this investigation, EnKF will be used to provide those estimates. Next, we will briefly present EnKF for data assimilation in dynamical systems.

2.3. Ensemble Kalman filter

In EnKF, first introduced by Evensen [Evensen (1994)] as an alternative to the extended Kalman filter for nonlinear dynamical systems, a finite number of Monte Carlo samples of the (augmented) state vector \mathbf{x}_k are propagated forward in time using the original model operator, treated as a black box model. One main concept behind the success of EnKF is that the statistical moments of the unknown state vector can be approximated using ensemble averaging. EnKF also performs a linear *analysis* or update step that is inherited from KF, essentially relying on second order moments (i.e. covariances). The linear analysis step offers computational efficiency but introduces errors in the estimated conditional pdf of \mathbf{x}_k since it ignored higher order moments in the target state pdf.

In one iterations of data assimilation using EnKF, we start with a prior pdf of \mathbf{x} given by $\mathbf{x}_k \sim p(\mathbf{x}_k^f)$. This prior pdf is the pdf of the state at time $t = t_k$ prior to assimilating the available data that is available at that time instance. This prior pdf is approximated using a set of Monte Carlo samples or trajectories of the state vector as provided through time-integration of the model operator. In the analysis step, EnKF estimates the conditional pdf $\mathbf{x}_{k(j)} \sim p(\mathbf{x}_{k(j)}^a)$ given the available vector of observations \mathbf{d}_j .

In summary, given model and measurement equations, as in Eqs. (6)-(7), EnKF provides Monte Carlo samples of the state vector *approximately* distributed according to the conditional pdf the state vector given available observations as follows [Evensen (2006)]. Start by constructing an initial ensemble $\{\mathbf{x}_{0,i}^a\}$ of size N with $i = 1, \dots, N$, using the prior pdf of \mathbf{x}_0 (prior to assimilating any data/observations). This prior pdf relates to the knowledge that is available relating to the initial conditions of the dynamical system. For each subsequent iterations, perform the following three steps

1. Forecast step: Repeat the time-integration

$$\mathbf{x}_{k,i}^f = \mathbb{U}(\mathbf{x}_{k-1,i}^a, \mathbf{f}_k, \boldsymbol{\zeta}_{k-1,i}), \quad i = 1, \dots, N \quad (9)$$

until observations are available for assimilation, where $\boldsymbol{\zeta}_{k-1,i}$ are Monte Carlo samples of the random vector $\boldsymbol{\zeta}_{k-1}$.

2. Analysis step:

$$\mathbf{d}_{j,i} = \mathbb{H} \mathbf{x}_{k(j),i}^f + \boldsymbol{\varepsilon}_{j,i}, \quad i = 1, \dots, N \quad (\text{perturbed observations}) \quad (10)$$

$$\bar{\mathbf{d}}_j = \frac{1}{N} \sum_{i=1}^N \mathbf{d}_{j,i}, \quad (11)$$

$$\bar{\mathbf{x}}_{k(j)}^f = \frac{1}{N} \sum_{i=1}^N \mathbf{x}_{k(j),i}^f, \quad (12)$$

$$\mathbf{P}_{xd} = \frac{1}{N-1} \sum_{i=1}^N \left(\mathbf{x}_{k(j),i}^f - \bar{\mathbf{x}}_{k(j)}^f \right) \left(\mathbf{d}_{j,i} - \bar{\mathbf{d}}_j \right)^T, \quad (13)$$

$$\mathbf{P}_{dd} = \frac{1}{N-1} \sum_{i=1}^N \left(\mathbf{d}_{j,i} - \bar{\mathbf{d}}_j \right) \left(\mathbf{d}_{j,i} - \bar{\mathbf{d}}_j \right)^T, \quad (14)$$

$$\mathbf{K}_{k(j)} = \mathbf{P}_{xd} \mathbf{P}_{dd}^{-1}, \quad (15)$$

$$\mathbf{x}_{k(j),i}^a = \mathbf{x}_{k(j),i}^f + \mathbf{K}_{k(j)} \left(\mathbf{d}_{j,i} - \mathbb{H} \mathbf{x}_{k(j),i}^f \right), \quad i = 1, \dots, N. \quad (16)$$

In general, the number of trajectories N is chosen to accurately capture the cross-correlation between the state forecasts and perturbed observations, as approximated by \mathbf{P}_{xd} in Eq. (13).

3. Application to Spectral Wave Modeling

In this section, we describe an application of the data assimilation framework to a case study involving an area offshore of Yakutat, Alaska. For data assimilation purposes, spooondrift wave measurement buoys were deployed off the coast of Yakutat, providing the observations to be fused with computational model forecasts as provided by SWAN numerical wave model [Booij, Ris and Holthuijsen (1999)].

3.1. Case Study

The data assimilation framework is applied to a case study involving an area offshore of Yakutat, Alaska, where the community is reliant on 100% diesel energy generation. The community, however, is considering utilizing renewable electricity generation, in particular wave energy. The University of Alaska Fairbanks (UAF) has completed a resource assessment using measurements and numerical modeling [Tschetter, Kasper and Duvoy (2016)]. A regional wave model was used in order to characterize the regional wave climate, and identify promising installation sites for WECs. It was found that the average annual wave energy at the site is around 20 kW/m, and could provide more electricity than Yakutat's electrical demand.

The coastal geography and offshore bathymetry in the area of interest are shown in Fig. 1. The baseline model setup for this analysis is taken from the UAF study [Tschetter et al. (2016)], which included a 10-year wave model hindcast. The coarse model domain is shown in Fig. 1 and the intermediate model domain is shown in Fig. 2. Additionally, the nearshore domain setup for data assimilation is shown in Fig. 2, which is rotated by 20 degrees to be approximately parallel to the shore.

Offshore of Yakutat, deployment operations limited the deeper Spotter buoy (SPOT-0397) deployment location to about 3 nautical miles offshore, which in turn determined the extent of this application's model domain considered for data assimilation. The two Spotter buoys that were deployed in 2020 (at 67m and 109m depths) are also shown in Fig. 2.

3.2. SWAN Numerical Wave Model

The SWAN model [Booij et al. (1999)] is a fully discrete spectral wave model which integrates the energy balance equation, describing the evolution of the wave spectrum in time, geographical

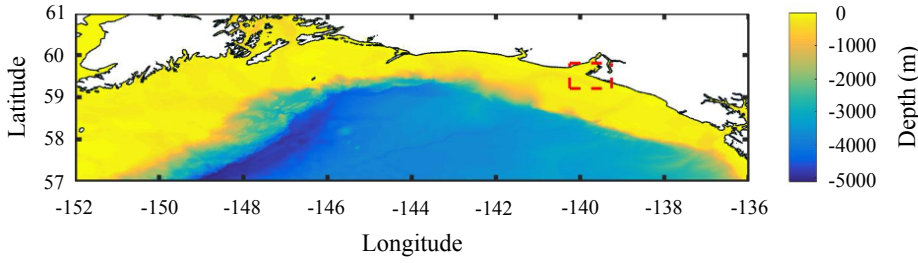


Figure 1: Coarse SWAN domain bathymetry. The outline of the intermediate SWAN domain is indicated by the red dotted line.

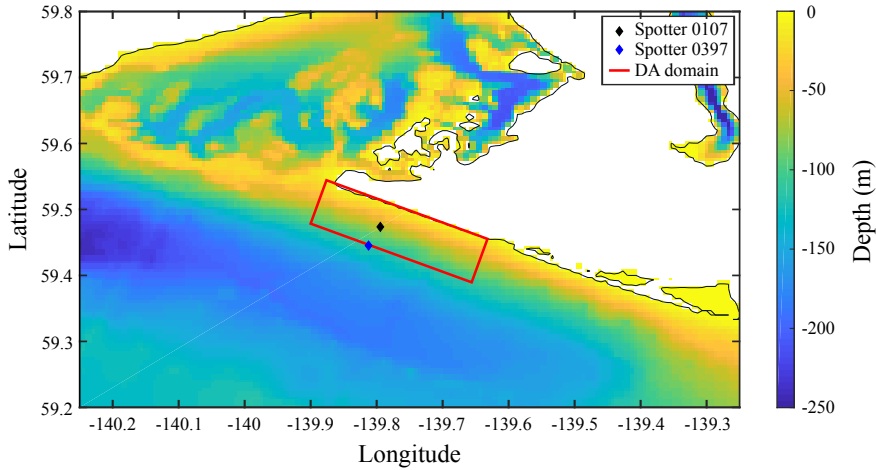


Figure 2: Intermediate SWAN domain showing the domain used in data assimilation and the location of the buoys providing observational data.

and spectral spaces (defined in SWAN by the relative radian frequency and the wave direction). The action density $N(\sigma, \theta)$ is equal to the energy density $E(\sigma, \theta)$ divided by the relative frequency σ , where θ is the wave direction. The evolution of the action density N is governed by [Komen, Cavaleri, Donelan, Hasselmann, Hasselmann and Janssen (1996)]:

$$\frac{\partial N}{\partial t} + \nabla_{\vec{x}} \cdot \left[\left(\vec{c}_g + \vec{U} \right) N \right] + \frac{\partial c_\theta N}{\partial \theta} + \frac{\partial c_\sigma N}{\partial \sigma} = \frac{S_{tot}}{\sigma}, \quad (17)$$

where $N(\sigma, \theta)$ is the action density, x is space, t is time, c_g represents propagation velocity of the action in geographical space, C_σ is propagation velocity in frequency space, c_θ is propagation velocity in wave directional-space. The source term, S_{tot} , in SWAN captures various sources of excitation and external effects, including the atmospheric (e.g. wind) input, whitecapping dissipation, and decay due to bottom friction. The integration of the action balance equation, Eq. (17), is accomplished with finite difference discretization in time, physical and spectral spaces. The SWAN model utilizes fully implicit numerical schemes.

3.3. Available data

For the data assimilation experiments, the available observations are in the form of two spectral bulk parameters, namely significant wave height and energy period, from the SPOT-0397 buoy near

the border of the computational domain (see Fig. 2). The significant wave height, H_s , and energy period, T_e , relate to the wave energy density as in

$$H_s = 4\sqrt{m_0}, \quad (18)$$

$$T_e = \frac{m_{-1}}{m_0}, \quad (19)$$

with the associated relevant spectral moments

$$m_0 = \int E(\omega, \theta) d\omega d\theta, \quad (20)$$

$$m_{-1} = \int \omega^{-1} E(\omega, \theta) d\omega d\theta, \quad (21)$$

at a particular time and spatial coordinate.

In the update step of EnKF, wave spectra over the domain were updated based on the difference in the two bulk parameters between the model predictions and the buoy data at the buoy location. The updated bulk parameters are subsequently used to update the discretized spectra using frequency and amplitude modulation as described in App. A. The data assimilation framework integrates the wave energy density in time to the nearest 10th minute forecast interval at which the next data is available for assimilation, and incorporates the data when updating the state and four parameters that control the BC correction.

3.4. Boundary Condition Correction

Our data assimilation framework attempts to not only update the unknown state vector (discretized wave spectra, or summary statistics thereof, over the computational domain), but also correct the boundary conditions provided by the larger-scale model simulations (nested SWAN runs over increasingly larger computational domain, shown in Fig. 1 and Fig. 2).

For the source of uncertainty in our computational model, we implemented a stochastic model for the boundary conditions which guarantees a certain level of uncertainty in the wave spectra along the boundary. This is achieved via amplitude and frequency modulation of the provided boundary condition (BC) spectra over space and time. To reduce the discrepancy between observations and SWAN model predictions, we rely on a correction of the prescribed boundary condition energy density, $E_{BC, \text{ nested}}$, given by

$$E_{BC, \text{ corrected}}(\omega, \theta, \vec{x}, t) = a_1(t) E_{BC, \text{ nested}}(a_2(t) \omega, \theta, \vec{x}, t) \quad (22)$$

with amplitude and frequency modulation factors, $a_1(t)$ and $a_2(t)$, respectively. The modulation factors follow an exponential decay/growth model with time-varying decay/growth rates, parametrized by a total of four unknown parameters, as in

$$a_i(t) = \exp(\alpha_i \exp(b_i(t)(t - t_{\text{ref}}))), \quad i = 1, 2, \quad (23)$$

$$b_i(t) = \frac{1}{2} (\beta_i + \gamma_1) (1 - \tanh(\gamma_2(t - t_{\text{ref}} - \tau))) - \gamma_1, \quad i = 1, 2. \quad (24)$$

The unknown parameters α_1 and α_2 control the initial values of the modulation factors a_1 and a_2 while β_1 and β_2 determine the initial values of the corresponding decay rates b_1 and b_2 (or

equivalently the initial gradient of the modulation factors). The time offset t_{ref} is chosen to be the last time at which data was assimilated. Therefore, for each modulation factor, we have introduced two degrees of freedom to control their initial values as well as their decay rates in time. By design, the modulation factors are strictly positive due to the first exponential operator in Eq. (23). Furthermore, the same factors are guaranteed to approach a value of one (i.e. no modulation) over longer time forecasts since the decay rate b converges to γ_2 (a positive constant) as shown in Eq. (24). Therefore, regardless of the values of the four parameters, the corrected BC spectra converge to the pre-specified ones for large time (roughly > 4 days) regardless of what the data suggests. This is achieved by choosing $\gamma_1 = 0.03$, $\gamma_2 = 0.05$, and $\tau = 24$ hours, with those values obtained using optimization experiments on simplified models. This modeling choice is based on the observation (through statistical studies, not shown for brevity) that any discrepancy in the BC spectral bulk parameters tend to persist on average for a couple of days.

In addition to correcting the state vector, comprised of two spectral bulk parameters (significant wave height and energy period) across all nodes in the computational domain, the four parameters that control the temporal behavior of the boundary condition amplitude and frequency modulation factors will also be updated using data assimilation by augmenting the state vector with the four unknown parameters. In a data assimilation context, we are thus performing joint state and parameter estimation. Since the assimilation of data reduces the uncertainty in those parameters (and subsequently the uncertainty in BC spectra) over time, we artificially inflate the variance of the unknown parameters while maintaining their mean values (using a linear transformation) to maintain a minimum allowable level of uncertainty. This minimum allowable standard deviations, 0.2 for α_i and 0.05 for β_i , were chosen based on numerical experiments using synthetic data in order to cause sufficient levels of uncertainty in the state for forecast purposes. Fig. 3 provides Monte Carlo realizations of the modulation factor $a(t)$ and associated decay rate $b(t)$ for parameters α and β with Gaussian distributions of zero mean. Furthermore, Fig. 4 provides Monte Carlo realizations of the modulation factor $a(t)$ for a Gaussian α parameter with a mean of -0.7 to illustrate the ability to capture an initial discrepancy in amplitude or frequency while also converging back to a modulation factor of 1 (i.e. no effective modulation). See [Khalil, Sarkar, Adhikari and Poirel (2015)] for a discussion on artificial inflation of parameter variance in data assimilation.

Strong cross-correlations across the entire state space were observed from Monte Carlo SWAN model simulations, suggesting that a small ensemble for EnKF would suffice in this context. It was determined that an ensemble of 10 to 20 model runs is sufficient to capture the statistical error characteristics in the state of the system. Therefore, we relied upon an EnKF ensemble size of 20 for all results included in this paper.

3.5. Data Assimilation Workflows

Coupling the previously described SWAN numerical wave model for forecasting, ensemble Kalman filter for data assimilation, along with the boundary condition corrections, we obtain workflows as shown in Fig. 5. The flowchart illustrates the interplay between key components such as the wave and boundary condition error models, the data assimilation forecast and analysis steps, and the available buoy data. The two modeling components, colored in blue, relate to the physics-based numerical wave model and the data-driven error model used in correcting the boundary conditions available from offline simulations involving nested SWAN simulations. This hybrid

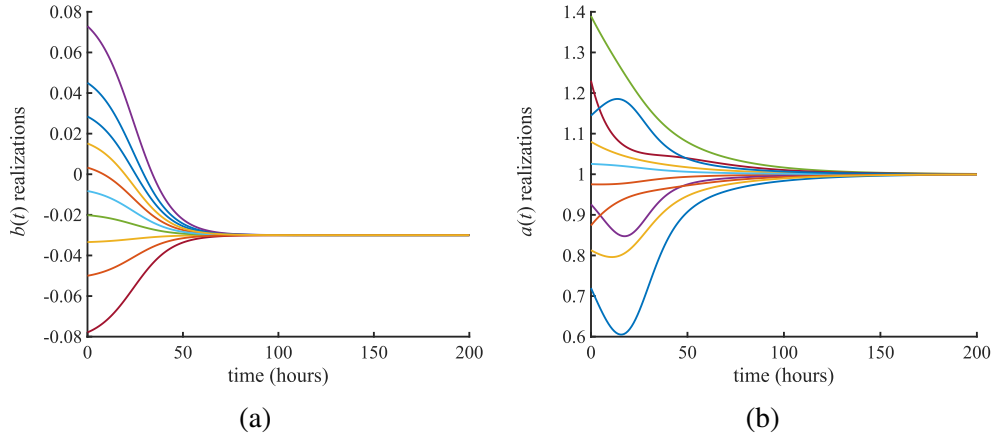


Figure 3: Ten Monte Carlo realizations of the modulation factor $a(t)$ and associated decay rate $b(t)$ for parameters α and β with means of zero and standard deviations of 0.2 for α and 0.05 for β

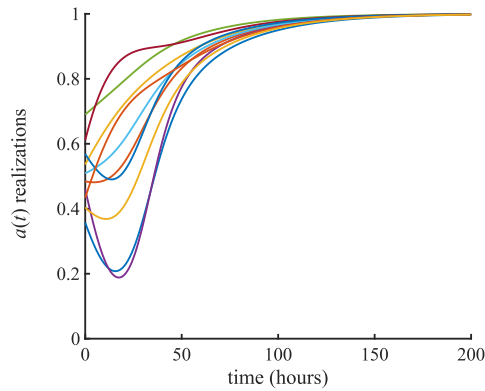


Figure 4: Ten Monte Carlo realizations of the modulation factor $a(t)$ for parameters α and β with means of -0.7 for α and 0 for β and standard deviations of 0.2 for α and 0.05 for β .

modeling approach, combining physics-based and data-based modeling strategies, results in greater accuracy of numerical wave forecasts.

4. Results and Discussion

A series of data assimilation experiments was performed using the Spotter buoy data from Yakutat, Alaska for the period of May 18 - September 23, 2020. For each experiment, first the nested SWAN runs described above were ran to obtain the baseline computational predictions. Then, EnKF was used to perform data assimilation for a six hours period, with data coming in about once per hour, followed by a 24 hour forecast starting from the corrected state. Six hours were found to be sufficient to mimic a long running data-assimilation scheme. The goal is to compare the baseline predictions to the forecasts into the future using data-assimilation. This forecast would be used to inform grid operations. The baseline prediction is based on the SWAN model driven by Wave Watch III conditions, which do incorporate wind data assimilation, but not the local data from the spotter buoy. The data from Spotter 0397 at the boundary was used for data assimilation,

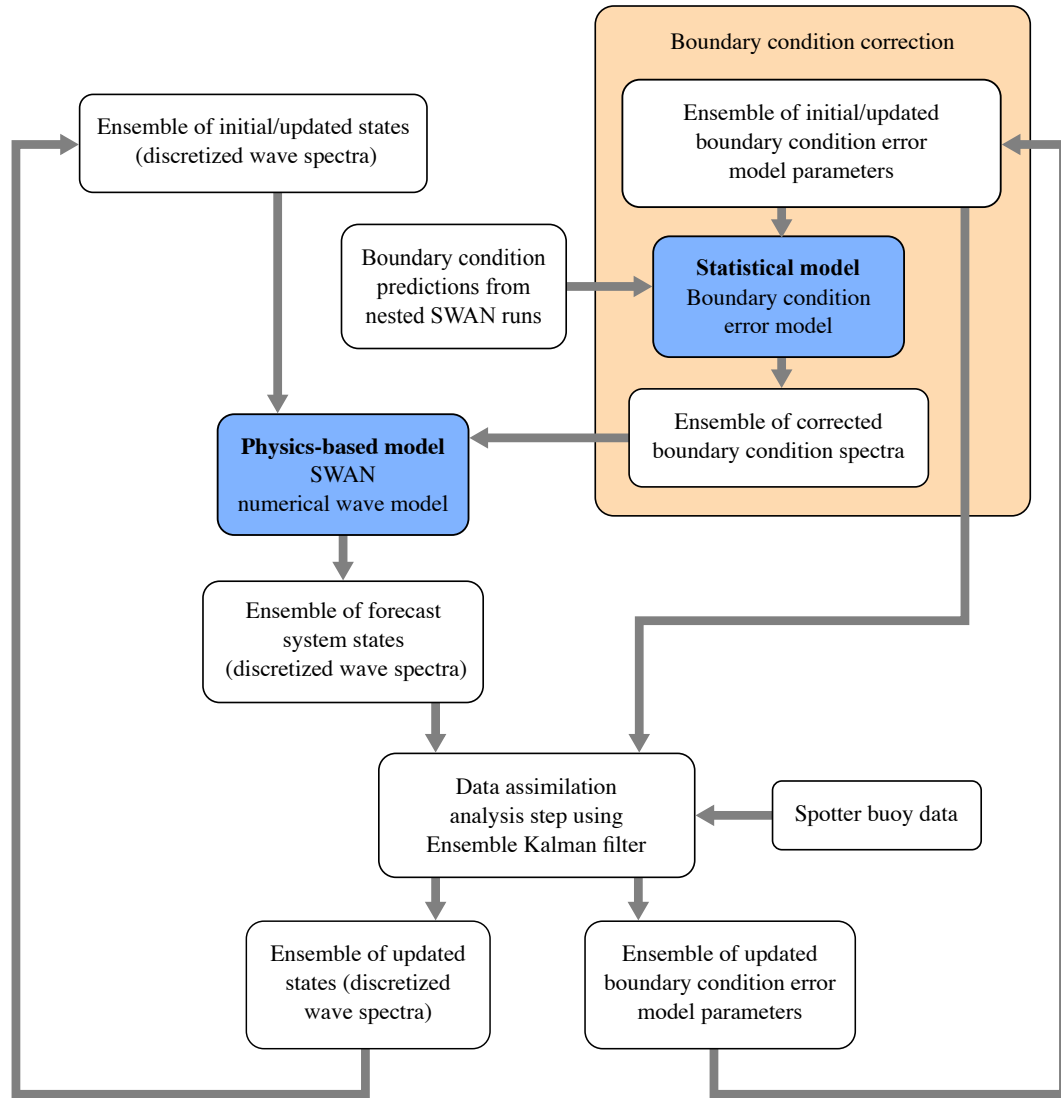


Figure 5: A schematic flowchart of the data assimilation framework as applied to the joint state and parameter inference for wave characteristic predictions.

while Spotter 0107 is considered the location of interest, i.e., where a WEC would be located. An example of one of these data assimilation experiments is shown in Fig. 6. It can be seen that the data-assimilated predictions start from the corrected state, follow the data trend for some period of time, and eventually return to the baseline prediction. This is the desired behavior enforced through the boundary condition model described above.

Similar experiments were performed every six hours for the period from May 18 - September 23, 2020, after removing missing (e.g. wind data was missing for several days in this period) or corrupt data. A total of 403 experiments were performed. We compare the 6-hour forecast at the location of the WEC, i.e., where Spotter 0107 (not used for data-assimilation) is located. Fig. 7 shows the RMSE for both the baseline and data-assimilation predictions for all experiments. The RMSE is calculated based on the norm of the error vector for the 6-hour period (i.e., the difference

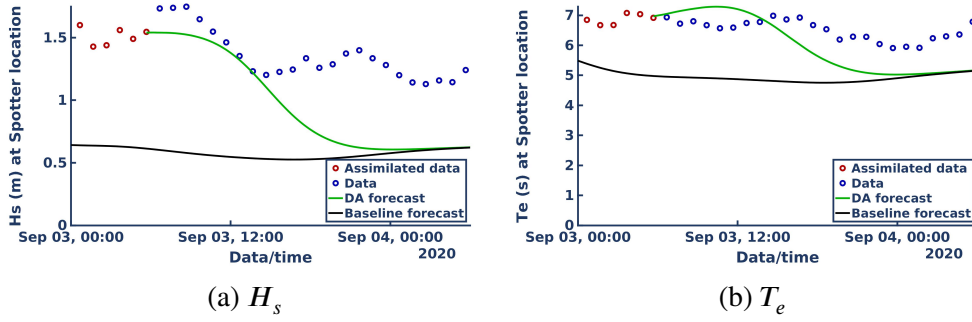


Figure 6: Single data-assimilation experiment for forecasting starting at 6am on September 3. Both H_s and T_e are shown at the measurement (Spotter 0397 at the boundary).

	baseline	with data assimilation
mean H_s RMSE	0.627 m	0.292 m
scatter (standard deviation) in H_s RMSE	0.390 m	0.290 m
mean T_e RMSE	1.32 s	0.711 s
scatter (standard deviation) in T_e RMSE	0.924 s	0.615 s

Table 1

Summary statistics for the predictive error (RMSE) from all experiments.

between prediction and measurement for all spotter observations in that period) as

$$RMSE = \frac{\|p - d\|}{\sqrt{N}}, \quad (25)$$

where p and d are the vectors of predictions and observation data, respectively, and N is the number of observations (length of p and d). It can be seen in Fig. 7 that the data assimilation significantly reduces the error in both H_s and T_e . Table 1 gives some summary statistics of the distributions shown in Fig. 7.

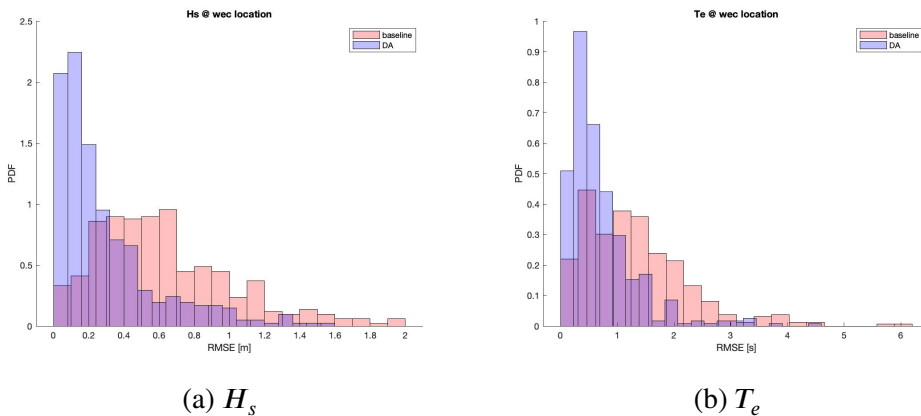


Figure 7: Comparison of predictive error (RMSE) in the forecast between the baseline and data-assimilation results at the proposed WEC location (Spotter 0107).

Although the implemented data-assimilation framework works as expected it can occasionally result in larger errors than the baseline. As an example, Fig. 8 shows a particularly bad case where the trend of the data changes significantly after data-assimilation is ended. The predictions are seen to follow the trend of the last 3 observations which would suggest the H_s and T_e are very rapidly increasing. The resulting predicted sea-states are nonphysical (e.g., H_s of more than 15m). To address these cases we capped the data-assimilation-based forecasting to twice the baseline prediction for H_s and 1.5 times the baseline prediction for T_e . The results shown in Fig. 7 and Fig. 9 use this capping. In future work, a more rigorous regularization technique could be used. Fig. 9 shows the results of all experiments (same results as in Fig. 7) as a relative error, i.e., the difference between the baseline and data-assimilation RMSE. While most values are positive—indicating an error reduction when using data-assimilation—it can be seen that for some of the experiments the data-assimilation resulted in increased error. This is more common for the T_e predictions. A more rigorous regularization should help reduce both the frequency and severity of these cases.

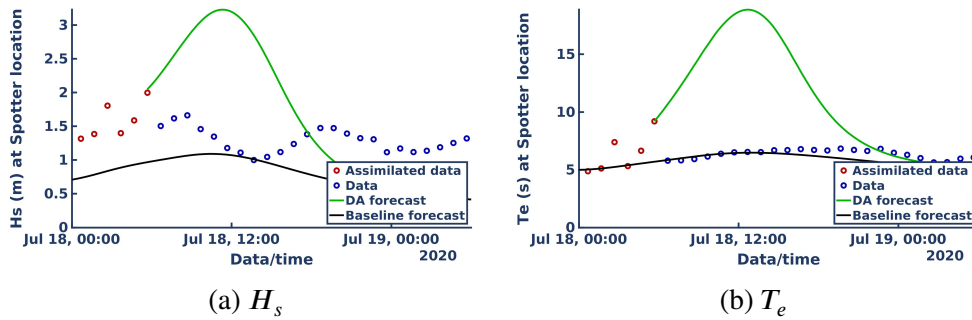


Figure 8: Single data-assimilation experiment for forecasting starting at 6am on July 18. Both H_s and T_e are shown at the measurement (Spotter 0397 at the boundary).

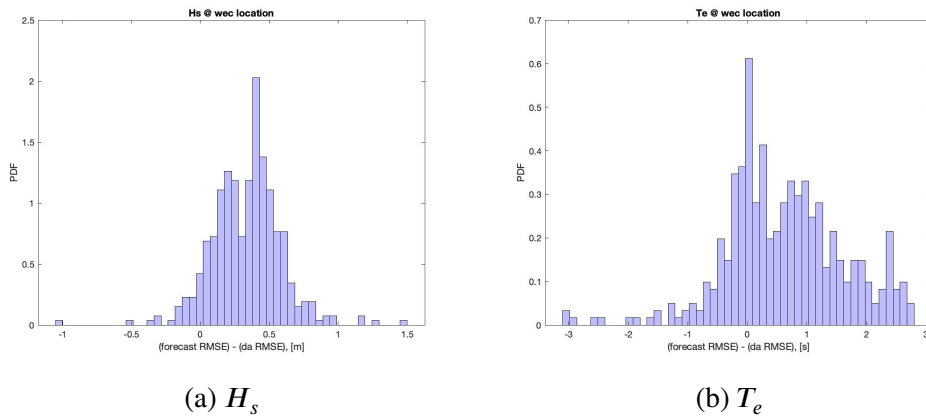


Figure 9: Relative error between the data-assimilation and baseline forecasts at the WEC location (Spotter 0107).

5. Conclusion

In this paper we presented the development and assessment of a wave modeling framework with real-time data assimilation capabilities for wave energy converter power prediction. Available real-time wave spectra from low-cost wave measurement buoys allowed for operational data assimilation with the ensemble Kalman filter technique within a hybrid modeling procedure whereby physics-based numerical wave models are combined with data-driven error models that aim to capture the discrepancy in prescribed boundary conditions. The measured wave spectra are assimilated for combined state and parameter estimation while taking into account model and observational errors. The analysis of incoming data allowed for more accurate and precise wave characteristic predictions at the locations of interest. Initial deployment data obtained offshore Yakutat, Alaska, indicated that measured wave data from one buoy that were assimilated into the wave modeling framework resulted in improved forecast skill in comparison to traditional numerical forecasts.

Acknowledgments

Chris Flanary at Integral Consulting, Inc., set up and ran the WaveWatchIII model, which provided boundary conditions into the coarse SWAN domain. Sandia National Laboratories is a multimission laboratory managed and operated by National Technology and Engineering Solutions of Sandia, LLC., a wholly owned subsidiary of Honeywell International, Inc., for the U.S. Department of Energy's National Nuclear Security Administration under contract DE-NA-0003525. The views expressed in the article do not necessarily represent the views of the U.S. Department of Energy or the United States Government.

A. Updating of Wave Energy Density to Match Spectral Parameters

Herein, we provide supplementary details to describe a particular transformation of 2D wave energy spectra with resulting bulk parameters matching target (pre-specified) values that are provided from the analysis step of EnKF. In particular, we will focus on two bulk parameters, namely the significant wave height and mean energy period. We will show how the transformation parameters can be obtained analytically using the starting and target bulk parameter values.

We start with a 2D wave energy spectrum, $E(\omega, \theta)$, with the associated relevant spectral moments

$$m_0 = \int E(\omega, \theta) d\omega d\theta, \quad (26)$$

$$m_{-1} = \int \omega^{-1} E(\omega, \theta) d\omega d\theta, \quad (27)$$

and relevant bulk parameters, namely significant wave height, H_s , and mean energy period, T_e , given by

$$H_s = 4\sqrt{m_0}, \quad (28)$$

$$T_e = \frac{m_{-1}}{m_0}. \quad (29)$$

This spectrum might be describing the wave characteristics at a particular computational node, whether along the boundary or inside the domain of interest. In data assimilation workflows, we

will often face the task of updating the wave spectra to match a "target" significant wave height and mean energy period. Let's denote those by \hat{H}_s and \hat{T}_e , respectively. We will use the following spectral transformation ¹ to arrive at those target values:

$$\hat{E}(\omega, \theta) = a_1 E(a_2 \omega, \theta) . \quad (30)$$

It can shown that the above transformation results in new spectral moments that can be related to the original one analytically using

$$\hat{m}_0 = a_1 a_2 m_0 , \quad (31)$$

$$\hat{m}_{-1} = \frac{a_1}{a_2} m_{-1} . \quad (32)$$

The above expression can be used to derive the new bulk parameters that correspond to the transformed spectrum:

$$\begin{aligned} \hat{H}_s &= 4 \sqrt{\hat{m}_0} \\ &= \sqrt{a_1 a_2} 4 \sqrt{m_0} \\ &= \sqrt{a_1 a_2} H_s , \end{aligned} \quad (33)$$

and

$$\begin{aligned} \hat{T}_e &= \frac{\hat{m}_{-1}}{\hat{m}_0} \\ &= \frac{\frac{a_1}{a_2} m_{-1}}{a_1 a_2 m_0} \\ &= \frac{1}{a_2^2} \frac{m_{-1}}{m_0} \\ &= \frac{1}{a_2^2} T_e . \end{aligned} \quad (34)$$

Equations (33) and (34) can be used to solve for the two unknown coefficients that are used in transforming the spectrum (see Equation (30)), resulting in the following amplitude and frequency modulation to achieve the target bulk parameter values.

$$a_1 = \left(\frac{\hat{H}_s}{H_s} \right)^2 \frac{\hat{T}_e}{T_e} , \quad (35)$$

$$a_2 = \sqrt{\frac{T_e}{\hat{T}_e}} . \quad (36)$$

¹There are other transformations that one might use. This particular choice guarantees physically valid spectra as long as the target bulk parameters are themselves physically valid.

References

- Andrieu, C., Doucet, A., 2003. Online expectation-maximization type algorithms for parameter estimation in general state space models, in: Proceedings of ICASSP '03, the IEEE International Conference on Acoustics, Speech, and Signal Processing, Hong Kong.
- Booij, N., Ris, R.C., Holthuijsen, L.H., 1999. A third-generation wave model for coastal regions: 1. model description and validation. *Journal of geophysical research: Oceans* 104, 7649–7666.
- Chui, C.K., Chen, G., 1999. *Kalman Filtering with Real-time Applications*. third ed., Springer, Berlin.
- Doucet, A., Godsill, S.J., Andrieu, C., 2000. On sequential Monte Carlo sampling methods for Bayesian filtering. *Statistics and Computing* 10, 197–208.
- Evensen, G., 1994. Sequential data assimilation with a nonlinear quasi-geostrophic model using monte carlo methods to forecast error statistics. *Journal of Geophysical Research: Oceans* 99, 10143–10162.
- Evensen, G., 2006. *Data Assimilation: The Ensemble Kalman Filter*. Springer, Berlin.
- Evensen, G., et al., 2009. *Data assimilation: the ensemble Kalman filter*. volume 2. Springer.
- Guedes Soares, C., Rusu, L., Bernardino, M., Pilar, P., 2011. An operational wave forecasting system for the portuguese continental coastal area. *Journal of Operational Oceanography* 4, 17–27.
- Kalman, R.E., 1960. A new approach to linear filtering and prediction problems. *Journal of Basic Engineering* 82, 35–45.
- Khalil, M., Sarkar, A., Adhikari, S., 2009. Nonlinear filters for chaotic oscillatory systems. *Journal of Nonlinear Dynamics* 55, 113–137.
- Khalil, M., Sarkar, A., Adhikari, S., Poirer, D., 2015. The estimation of time-invariant parameters of noisy nonlinear oscillatory systems. *Journal of Sound and Vibration* 344, 81–100.
- Kitagawa, G., 1998. A self-organizing state-space model. *Journal of the American Statistical Association* 93, 1203–1215.
- Komen, G.J., Cavaleri, L., Donelan, M., Hasselmann, K., Hasselmann, S., Janssen, P., 1996. *Dynamics and modelling of ocean waves*.
- Ristic, B., Arulampalam, S., Gordon, N., 2004. *Beyond the Kalman Filter: Particle Filters for Tracking Applications*. Artech House, Boston.
- Rusu, E., Raileanu, A., 2016. A multi-parameter data-assimilation approach for wave prediction in coastal areas. *Journal of Operational Oceanography* 9, 13–25.
- Tanizaki, H., 1996. *Nonlinear Filters: Estimation and Applications*. second ed., Springer, Berlin.
- Tschetter, T., Kasper, J., Duvoy, P., 2016. Yakutat area wave resource assessment. Alaska Center for Energy and Power, Alaska Center for Energy and Power .